# Optimization and Computational Approach to Understand the Adsorption Behavior of Alizarine Red S on the Surface of Fish Scales

**Abdelmajid Regti [1,2,\*], Zouhair Lakbaibi [3], Hicham ben elayouchia [1], Mohammadine El Haddad [1], My Rachid Laamari [1], Adil Jaafar [4], Ilham Elazhary [1], Mamoune El Himri [1]**

[1] Laboratory of Analytical and Molecular Chemistry (LCAM), Poly-disciplinary Faculty of Safi, Cadi Ayyad University, BP 4162, 46000 Safi, Morocco
[2] Faculty of Applied Sciences-Ait Melloul - Ibn Zohr University, Agadir, Morocco
[3] Laboratory of Materials Engineering, Natural Resources and Environment (LMENRE), Faculty of Sciences and Techniques Errachidia, My Ismail University, BP 509 Boutalamine, Errachidia, Morocco
[4] Higher School of Education and Training, Berrechid, Hassan First University, Settat, Morocco
\* Correspondence: abdelmajid.regti@gmail.com;

Scopus Author ID 57204952778

**Abstract:** The key components of fish scales are hydroxyapatite and collagen, which form a natural composite. In this present study, fish scales were used as biosorbent to uptake Alizarine Red S dyes from the wastewaters. Here, dye concentration, adsorbent amount, pH, and temperature were optimized using complete factorial design analysis. Sixteen experiments were required, and a linear mathematical model representing the influence of the different variables and their interactions was obtained. The discussion covered analysis of variance (ANOVA), normal probability plots of residuals, and surface plots. Theoretical calculations by Metropolis Monte Carlo (MC) methods, the density functional theory (DFT), and the electrostatic potential surface (ESP) analysis were achieved to obtain a more understanding of the dyes adsorption mechanism on both collagen and hydroxyapatite (HDA) surfaces. The findings results exhibited that the ARS dye presents more tendency of adsorption on the collagen than on the HDA surface.

**Keywords:** biosorbent; complete factorial design; density functional theory; electrostatic potential surface; Metropolis Monte Carlo method.

## 1. Introduction

Dyeing effluents from several industrial sectors, mainly chemical textile finishing, are generally considered pollutants compounds [1-8]. Alizarin Red S is a durable anionic molecule from the anthraquinone family. In the textile industry, it is widely used as a dye. [9]. This dye can also be used to stain mineralized vertebrate bones, small invertebrate embryos, and other biological specimens [10]. Because this synthetic dye is a strong oxidizing agent, it must be kept away from heat and humidity [11]. It is resistant to degradation due to its structure, which provides high thermal, optical, and physical-chemical stability [12]. Hence, treatment studies focus on developing easy, simple, and effective processes for their safe and economical removal. Therefore, the effective removal of this toxic dye from sewage before it is discharged into the environment is very important and necessary.

Several strategies are currently widely used to remove harmful dyes from wastewater, such as physicochemical processes, including coagulation-flocculation, oxidation, membrane

filtration, and absorption [13, 14]. Among these, the adsorption process is promising and the most effective strategy due to its simplicity, low cost, and technical feasibility [15-20]. In particular, several researchers have introduced fish scales biomasses for dye removal from water and reduced the operational costs of adsorption processes [21-25]. Fish scales are tiny solid plates attached to the fish skin to protect its body and contain numerous valuable organic and inorganic components, mainly collagen and hydroxyapatite. It was evaluated that yearly, the fish preparing industry generates between 18 and 30 million tons of fish wastes, of which 4% are fish scales [26], which are considered waste materials with little commercial value but are useful for removing dyes from aqueous solutions. Fish scales are rich in fibrous protein, type I collagen, and hydroxyapatite. These two kinds could interact strongly with dyes molecules and, several studies confirm this observation [21-23]. Type I collagen takes on a helical conformation known as a "collagen helix" due to two amino acid sequence characteristics. These characteristics include high amino acid content and the presence of Glycine residues in every three positions. The first feature includes a sequence (Gly-X-Y)n, where X and Y are amino acid residues, but Proline and its post-translational modification, 4-hydroxyproline (Hyp), are commonly found in fish scales. Therefore, the most typical sequence to represent Type I collagen's amino acid sequences characteristics is the unit Gly-Pro-Hyp [27, 28]. The collagen unit and its protonated form (Collagen-H+) were optimized and exposed in Figure 1.
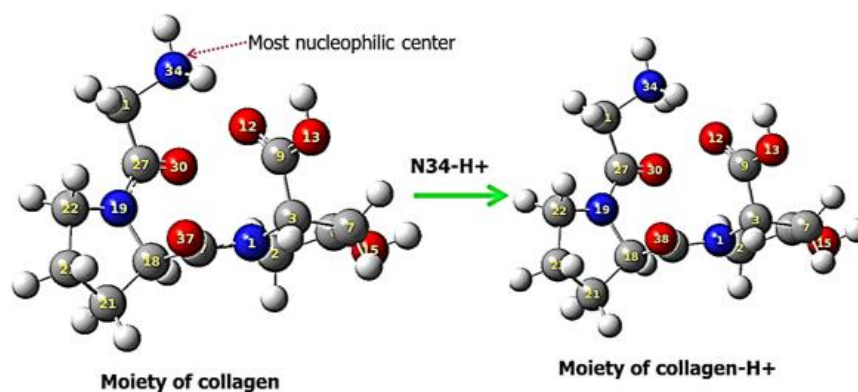


**Figure 1**. Optimized structures. Most nucleophilic center of the moiety of collagen was determined in term of Mulliken atomic spin density (MASD) analysis using nucleophilic Parr functions P+.

The optimization calculations were confirmed by the presence of zero negative frequency in the z-matrix.

Optimization of the treatment process is the needed fundamental mission for researchers. However, minimizing the number of experiments is required for decreasing the cost, the consumed period, and the environmental effect.

**Table 1.** Factors and levels used in the factorial design study.

| Parameter name study | Code | Low (-1) | High (+1) |
|---|---|---|---|
| pH | A | 2 | 12 |
| Adsorbent dosage (g/L) | B | 5 | 15 |
| Solution concentration (mg/L). | C | 25 | 50 |
| Température (K) | D | 293 | 323 |

The design of experiments is a commanding procedure that could accomplish to optimize the treatment process. It illustrates the variations of the response (efficiency or removal) as a function of variables to investigate the individual and their interaction effects for the alizarine Red S removal onto fish scales. In this study, the analysis of data and design of
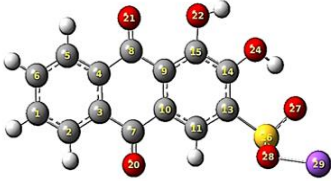
experiments was performed by analyzing the complete factorial design method. Table 1 displays four independent variables at two levels of high (+1) and low (-1): pH, biosorbent dose, concentration, and temperature (-1).

MC, DFT, and ESP calculations were used to evaluate the alizarine red S (ARS) adsorption behavior on both collagen and HDA surfaces. This computational finding allows supporting highlights to understand the adsorption process of ARS dye to the two studied surfaces. The adsorption behavior was carried in three environments (neutral media: NM, acidic media: AM, and basic media: BM). Indeed, the MC study makes it possible to compare the adsorption power of ARS with respect to each of the two studied surfaces for three media (NM, AM, and BM). The MC study appeared that the ARS is more adsorbed at the collagen surface than onto the HDA surface. Furthermore, we noticed that the acidic media favors the adsorption of ARS on the collagen than the other two media (NM and BM). For the second time, we are interested in studying and discussing the adsorption of ARS dye on the protonated and non-protonated form of collagen using DFT and ESP investigations.

## 2. Materials and Methods

Fish scales were obtained from a fish factory in Laayoune city (Morocco). The fish scales were first washed to remove the adhering dirt and then dried for several days. The dried scales were ground to a fine powder using a grinder and sieved. The resulting material was abbreviated as PFS (powdered fish scales). Alizarine Red S (ARS) used in this study was obtained from Aldrich. The optimized structure and some dye properties are shown in Table 2. A 500 ml of Colored solution was obtained by dissolving the required amount of dye in distilled water. Biosorption studies for evaluating PFS biosorbent for removing ARS dye from aqueous solutions were carried out using a batch method.

**Table 2.** General characteristics of ARS.

| Usual Name | Chemical structure | Type dye | CI Number | Molecular weight (g/mol) | λmax (nm) |
|---|---|---|---|---|---|
| Alizarin Red S |  | Anionique | 58 005 | 342.26 | 520 |

In this study, the analysis of data and design of experiments were performed by using full factorial design. Thus, the biosorption experiments were carried out with an initial dye concentration range from 25 to 50 mg/L, amount of PFS from 5 to 15 g/L, pH from 2 to 12, and temperature from 293K to 323K. The pH was adjusted to a given value by the addition of 1 mol/L of HCl or NaOH and was measured using a pH-Meter HANNA 5222. All dye solutions were centrifuged, and the concentrations of dyes were determined from their UV-Vis absorbance characteristic with the calibration method. A JENWAY 6300 UV/Visible spectrophotometer was used. The experimental design results were analyzed using statistical software (DESIGN EXPERT 12) to evaluate the effects and the statistical parameters.

The adsorbed quantity $q_e$ (mg/g) and the percentage removal of ARS on PFS were calculated using formula (1) and (2):

$$q_e = \frac{C_0 - C_e}{W}V \tag{1}$$

$$\mathrm{Re}\,moval \cdot Efficiency.\% = \frac{C_0 - C_e}{C_0}\,x100 \qquad (2)$$

where $C_e$ (mg/L) is dye concentration at equilibrium state, $C_0$ (mg/L) is the dye solution's initial concentration. V is the volume of the solution (L), and W is the mass of the biosorbent (g).

Adsorption simulation of ARS onto collagen and HDA as periodic surfaces (simulation box of 17.89×17.89×38.34 Å) in neutral media (100 of $H_2O$), acidic media (100 of $H_2O$, $20H_3O^+$ and $20Cl^-$), and basic media (100 of $H_2O$, $20OH^-$ and $20Na^+$) was explored using adsorption locator module and the COMPASS II force field integrated to the Materials studio version 8 program package [29].

The optimized geometries such as the collagen, collagen-H+, and ARS dye were performed using the DFT method [30], combined to the basis 6-311G++(d,p) [31] and the functional B3LYP [32] utilizing Gaussian 09 software [33]. As for (111), surface optimization of HDA is obtained employing Gaussian 09, which is integrated into Material studio Biovia version 8.0 at the same basis and function cited above. For both collagen and collagen-H+, the distribution densities of HOMO (occupied molecular orbital) and LUMO (low unoccupied molecular orbital) were produced. Then, we have calculated quantum parameters (QPs) such as the energy of HOMO ($E_{HOMO}$), the energy of LUMO ($E_{LUMO}$), the energy gap $\Delta E_g$ between $E_{HOMO}$ and $E_{LUMO}$ energies ($\Delta E_g = E_{LUMO} - E_{HOMO}$) [34] and the global chemical potential $\mu$ ($\mu = 0.5(E_{HOMO} - E_{LUMO})$ [35, 36]. Additionally, the reactive centers of the two form of collagen were estimated from three approaches as the analysis of spreading of HOMO and LUMO densities (DFMO), the analysis of electrostatic potential (ESP) on which: the red color signifies a strong negative electrostatic potential (EP); yellow (Moderately negative EP); blue (strong positive EP) and green (moderately positive EP) [37].

## 3. Results and Discussion

### 3.1. Characterization of PFS biosorbent.

The PFS structure was characterized in studies that include a non-mineralized organic component (type I collagen) and the mineralized inorganic component hydroxyapatite [38].Figure2 shows a band near 1040 $cm^{-1}$ due to the asymmetric stretching mode of vibration for the $PO_4$ group. The band at 610 $cm^{-1}$ is caused by the P–O vibrational band, which also provides hydroxyapatite evidence. In addition, IR absorption bands of N-H stretching (at 3418 $cm^{-1}$) are attributed to primary and secondary amides, and an IR absorption band from C=O bending (at 1646 $cm^{-1}$) is attributed to a primary amide. The results indicate that PFS also contained type I collagen as well as hydroxyapatite.

The XRD diagram of PFS (Figure 3) shows several broad peaks. The broadest peak at the diffraction angle 2θ of 32.5° is the result of the merger of three peaks corresponding to (211) (112) and (300) Miller plans of hydroxyapatite [39]. The peaks at the diffraction angles 2θ of 26.5°, 40°, 50° and 53° correspond to the (002), (310), (213), and (411) Miller plans of hydroxyapatite. This set of peaks is identical to the powder XRD pattern of hydroxyapatite (from diffraction Crystallography Open Database), which is also reported elsewhere [40].
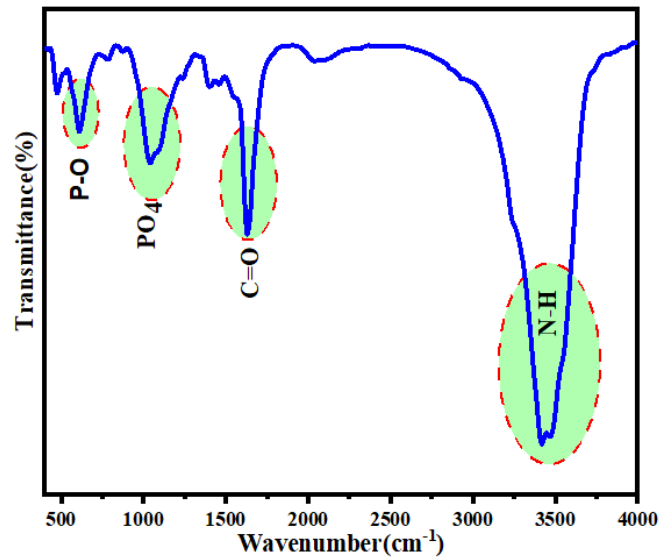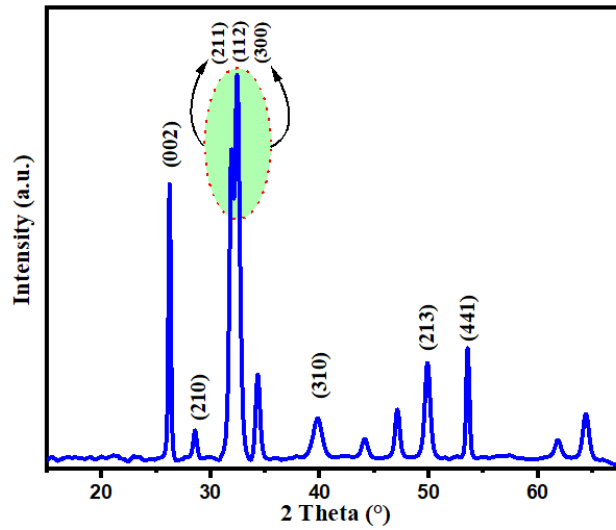
**Figure 2**. The FTIR spectra of PFS.
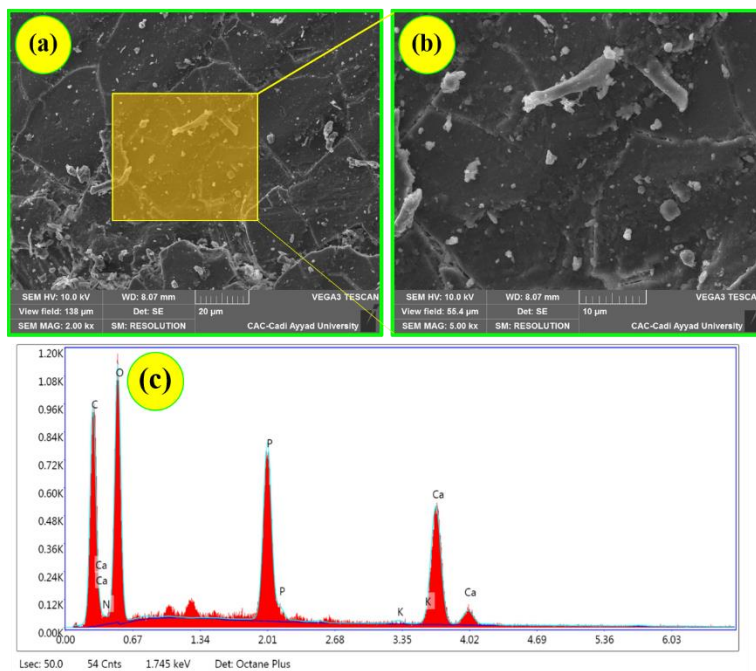


**Figure 3.** The XRD diagram of PFS



**Figure 4**. (**a-b**) The surface morphology of PFS; (**c**) EDS analysis of PFS.

The surface morphology of PFS is shown in Figure 4 (a-b). The fish scales have a smooth surface and look like jelly, which can be collagen. Many fibers are also observed. Information about elemental identifications and quantitative compositions of the biosorbents were obtained by EDS. The results of the elemental analysis are given in Figure 4(c). The presence of Ca, P, C, O, and N in the biosorbent is confirmed by semi-quantitative EDS analysis. The molar ratio of Ca/P in PFS is 1.56, and it agrees with the calculated value of 1.66 for hydroxyapatite $Ca_{10}(PO_4)_6$ $(OH)_2$. Characterizations of PFS confirm the presence of collagen Type I and hydroxyapatite.

### 3.2. Development of regression model equation for the dye removal.

Table 3 shows the design matrix with the response factorial method in two levels for the four variables studied. Sixteen tests were performed, along with the experiments' obtained results and predicted by the model and residuals. Figure 5 illustrates the results of the probability of the data being normal versus the studentized residual values. The residuals' probability distribution analysis with a 95% confidence shows that the data obtained from the experiments have a normal distribution.

**Table 3.** Factorial design matrix of four variables along with experimental and predicted responses for ARS removal by PFS.

| Run no | Coded values of independent variables | | | | ARS removal % | | |
|---|---|---|---|---|---|---|---|
| | A (pH) | B (dose) | C (con) | D (T) | Observed | Predicted | Residual |
| 1 | 1 | 1 | -1 | 1 | 4,12 | 4,15 | -0,0325 |
| 2 | 1 | -1 | 1 | 1 | 2,80 | 3,11 | -0,3125 |
| 3 | -1 | 1 | 1 | 1 | 78,20 | 78,44 | -0,2400 |
| 4 | -1 | -1 | -1 | -1 | 63,55 | 64,89 | -1,34 |
| 5 | 1 | -1 | -1 | 1 | 2,69 | 3,20 | -0,5075 |
| 6 | 1 | -1 | 1 | -1 | 3,25 | 3,00 | 0,2475 |
| 7 | -1 | -1 | 1 | -1 | 50,61 | 48,38 | 2,23 |
| 8 | -1 | 1 | 1 | -1 | 61,93 | 64,23 | -2,30 |
| 9 | -1 | -1 | 1 | 1 | 62,90 | 62,59 | 0,3075 |
| 10 | 1 | 1 | -1 | -1 | 3,17 | 3,96 | -0,7875 |
| 11 | -1 | 1 | -1 | -1 | 82,14 | 80,74 | 1,40 |
| 12 | -1 | -1 | -1 | 1 | 77,90 | 79,10 | -1,20 |
| 13 | -1 | 1 | -1 | 1 | 96,08 | 94,95 | 1,13 |
| 14 | 1 | -1 | -1 | -1 | 3,66 | 3,09 | 0,5725 |
| 15 | 1 | 1 | 1 | 1 | 4,92 | 4,07 | 0,8525 |
| 16 | 1 | 1 | 1 | -1 | 4,01 | 4,04 | -0,0325 |

The potential effect of each factor for removing alizarine red S was determined by the analysis of variance (ANOVA) in Table 4. The model obtained with an F-value of 1203.89 and P-value less than 0.0001, $R^2$ =0.9991, and Adjusted R-Squared = 0.9982, indicating a reliable model for the prediction of efficiency of ARS removal by PFS [41]. The Adequate precision for the ANOVA was obtained to be 84.41, which is a favorable value. The preferred value for adequate precision is >4 [42]. The sum of squares (SS) quantifies the importance of each factor in the adsorption process. The value of SS increases as the factor's significance increases. Each factor's main effects and interaction effects having a P value<0.05 are considered potentially significant.
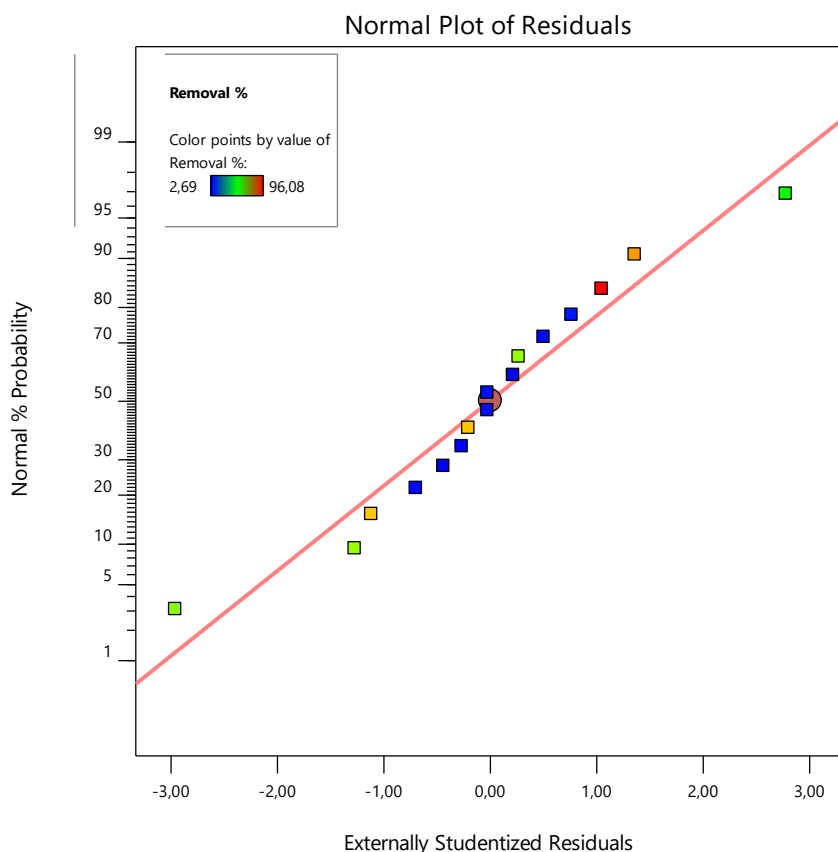
**Figure 5.** Normal probability of internally studentized residuals.

**Table 4.** Analysis of variance for the selected factorial model.

| Source | SS | DF | MS | F Value | P Value |
|---|---|---|---|---|---|
| Model | 19996,0844 | 7 | 2856,58348 | 1203,89352 | < 0.0001 |
| A-pH | 18542,9498 | 1 | 18542,9498 | 7814,83793 | < 0.0001 |
| B-PFS dose | 282,324006 | 1 | 282,324006 | 118,984109 | < 0.0001 |
| C-ARS Concentration | 275,311056 | 1 | 275,311056 | 116,028534 | < 0.0001 |
| D-Temperature | 205,134006 | 1 | 205,134006 | 86,4527507 | < 0.0001 |
| AB | 221,786556 | 1 | 221,786556 | 93,4708887 | < 0.0001 |
| AC | 269,698506 | 1 | 269,698506 | 113,663152 | < 0.0001 |
| AD | 198,880506 | 1 | 198,880506 | 83,8172429 | < 0.0001 |
| Residual | 18,9823 | 8 | 2,3727875 | | |
| Cor Total | 20015,0667 | 15 | | | |

R-Squared = 0.9991 ; Adjusted R-Squared = 0.9982; Adequate precision = 84,41 ;CV=4.09

The coded mathematical model of all possible combinations of studied factors A, B, C, and D can be given as:

$$Y = a_0 + a_1 A + a_2 B + a_3 C + a_4 D + a_5 AB + a_6 AC + a_7 AD + a_8 BC + a_9 BD + a_{10} CD + a_{11} ABC + a_{12} ABD + a_{13} ACD + a_{14} BCD + a_{15} ABCD. \tag{3}$$

where Y is the theoretical removal efficiency of ARS, $a_0$ is the global mean; $a_i$ and $a_{ij}$ are the regression coefficients of the effects factors and interactions, respectively. Coefficients factors that are statistically significant are replacing in the full factorial design model. The following model was obtained as a predictive model of ARS removal efficiency.

$$\textbf{Removal\%} = +37.62 - 34.04A + 4.20B - 4.15C + 3.58D - 3.72AB + 4.11AC - 3.53AD \tag{4}$$

The pH (A) had the greatest effect on removal efficiency, followed by PFS dose (B) and concentration(C); ph-solution concentration interaction (AC) is the most interaction that

affects the adsorption process but less than the effect of pH. Figure 6 shows a good agreement between the predicted and experimental results. The coefficient of variation (C.V% = 4.09) is low, which demonstrated clearly that the deviations between actual and predicted values were low and affirmed the precision and reliability of conducted experiments.
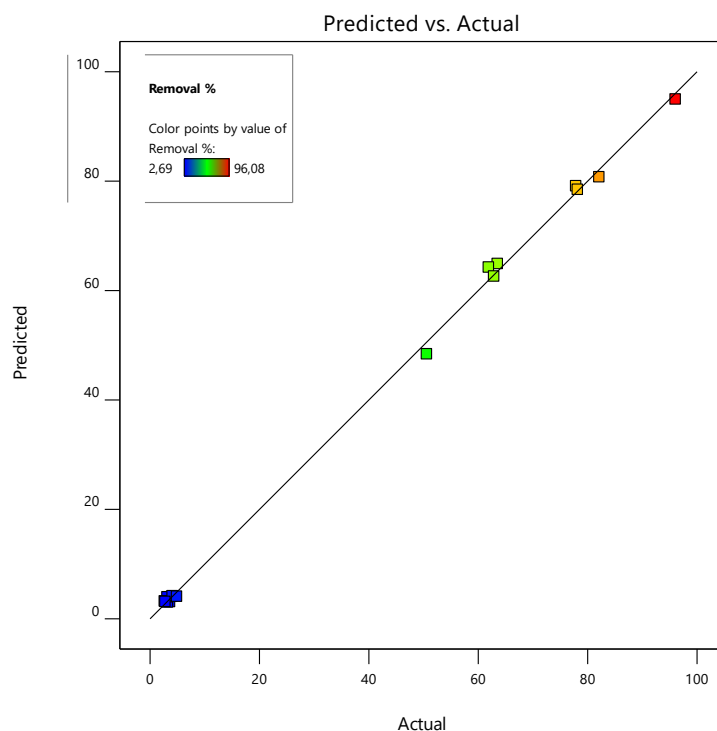


**Figure 6.** The plot of predicted versus experimental decolorization efficiency.

### 3.3. Estimation of quantitative effects and interactions.

It can be observed from the analysis of the coefficients of Eq. (4) that the pH was the most important variable of the adsorption process because of the largest value of the coefficient. The negative sign of this coefficient means that the removal efficiency was favored at low pH values. Figure 7 shows the response surface plot of the interaction effect of the pH factor, dose, temperature, and concentration on ARS removal efficiency. As can be observed, the highest dye removal efficiency is obtained at pH=2, and by increasing the pH, the removal percentage decreases. It can also be concluded that at pH=2, the dye removal efficiency was affected by temperature and initial concentration, while at basic pH, no influence from these parameters on the adsorption process was observed, showing a major effect of pH.

### 3.4. Thermodynamic parameters of biosorption

Temperature is a parameter that has been studied extensively in the literature and has an effect on the biosorption process [43]. The following equations determine the thermodynamic parameters related to the biosorption process ($\Delta G^0$, KJ/mol), enthalpy change ($\Delta H^0$, KJ/mol), and entropy change ($\Delta S^0$, J/mol K):

$$\Delta G^0 = -RTLn(K_C) \qquad (5)$$

where $\Delta G^0$ is the free energy change (KJ/mol), R is the universal gas constant (8.314 J/mol K), T is the absolute temperature (K), and $K_C$ states the equilibrium constants ($q_e/C_e$). The values of $\Delta H^0$ and $\Delta S^0$ can be calculated from the following equation:

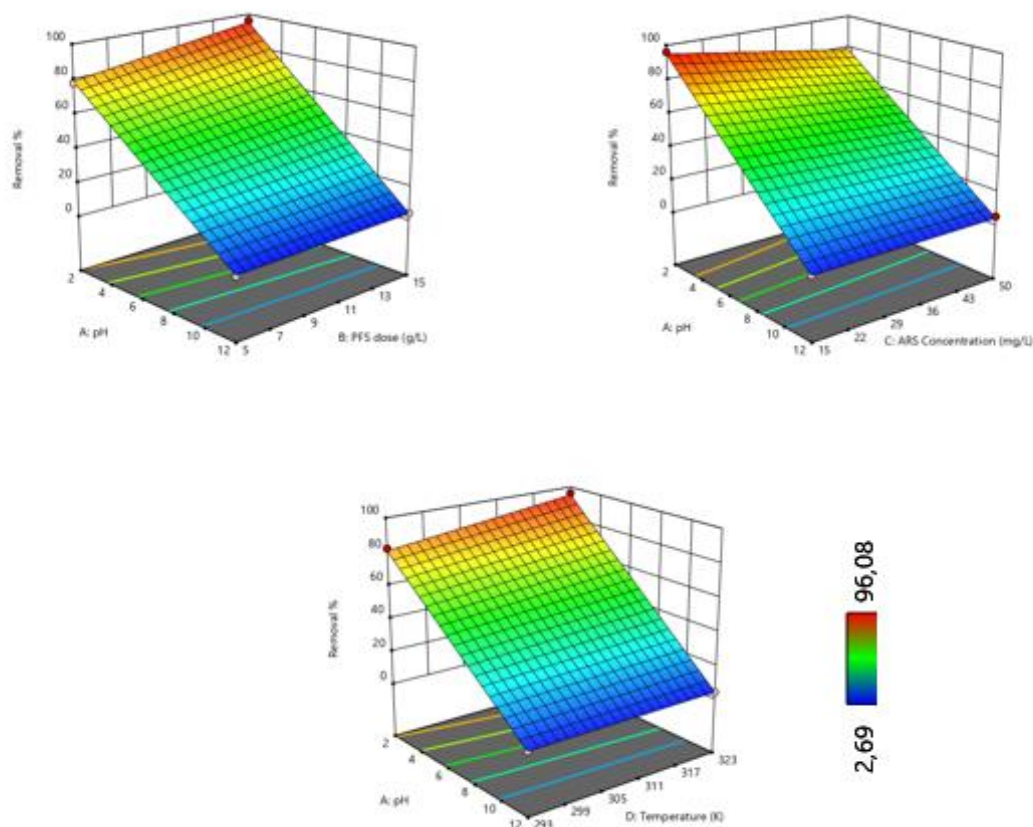$$Ln(K_C) = -\frac{\Delta H^0}{RT} + \frac{\Delta S^0}{R} \qquad (6)$$



**Figure 7**. 3D plots for interaction effects for ARS removal efficiency.

In order to test the ability of PFS biosorbent to remove ARS from aqueous solutions, we have carried out the evaluation of temperatures. Data were collected at different temperatures 293 K, 303 K, 313 K, and 323 K. The $\Delta H0$ and $\Delta S0$ values of dye obtained from the slope and intercept of Van't Hoff plots are presented in Table 5. The value of enthalpy $\Delta H0$ is 18.17 KJ/mol. This positive value indicates that the biosorption onto PFS was endothermic in nature. The positive value of $\Delta S0$ shows the increased disorder and randomness at the solid-solution interface of ARS with PFS biosorbent. The negative values of $\Delta G0$ show that the biosorption is favorable and spontaneous.

**Table 5.** Thermodynamic parameters for the biosorption of ARS onto PFS biosorbent.

| Temperature | Alizarine Red S | | |
| --- | --- | --- | --- |
| | ΔG0 (J/mol) | ΔH0 (KJ/mol) | ΔS0 (J/mol K) |
| 293 K | - 1220.86 | | |
| 303 K | - 2196.91 | 18.17 | 65.07 |
| 313 K | - 2847.61 | | |
| 323 K | - 3498.31 | | |

*3.5. Biosorption isotherms.*

The biosorption isotherms' significance because they show how the adsorbate solutes are distributed between the solution and the biosorbent at the equilibrium conditions. The

Langmuir and Freundlich isothermal models are the most widely used to fit experimental data. The Langmuir adsorption model is based on the assumptions of uniformly energetic adsorption sites, monolayer coverage, and no lateral interactions between adsorbed molecules. Langmuir's [44] mathematical linear form expression is as follows:

$$\frac{C_e}{q_e} = \frac{1}{K_L Q_0} + \frac{C_e}{Q_0} \tag{7}$$

where $q_e$ (mg/g) is the adsorbed amount at equilibrium, $C_e$ is the equilibrium concentration of the adsorbate (mg/L), $K_L$ is Langmuir equilibrium constant (L/mg), and $Q_0$ the maximum adsorption capacity (mg/g). The dimensionless constant called the equilibrium parameter, RL, could be used to express the essential characteristic of the Langmuir isotherm.

$$R_L = \frac{1}{1 + K_L C_0} \tag{8}$$

where $C_0$ is the initial dye concentration (mg/L). $R_L$ values indicate the adsorption is irreversible ($R_L = 0$), favorable ($0 < R_L < 1$), unfavorable ($R_L > 1$) [45]. The Freundlich isotherm confirms the surface's heterogeneity and that adsorption occurs at various adsorption energies at different locations. The adsorption energy varies depending on the surface coverage [46]. A linear mathematical expression of Freundlich isotherm was as follows:

$$\log q_e = \log K_F + \frac{1}{n} \log C_e \tag{9}$$

where $K_F$ (L/mg), Freundlich constant is related to adsorption capacity and *n*, the heterogeneity factor, while the *1/n* value is related to the adsorption intensity, isotherm model is favorable if ($0 < 1/n < 1$) or unfavorable ($1/n > 1$).

Table 6 summarizes both Langmuir and Freundlich isotherm data for ARS. Comparing the regression coefficient values for both the Langmuir and Freundlich isotherms at various temperature ranges between 293K and 323K, it was demonstrated that the Freundlich isotherm was the most appropriate isotherm to describe the equilibrium data for dyes biosorption onto PFS, as indicated by the high $r^2$. The value of parameter 1/n of the Freundlich equation gives an indication of the validity of the adsorption of the adsorbent- adsorbate system. The values of 1/n presented in Table 6 are between 0 and 1, suggesting that the adsorption of the ARS dyes on PFS is favorable.

**Table 6.** Isotherms parameters of the biosorption of Alizarin Red S onto PFS biosorbent.

| | Alizarin Red S | | | |
|---|---|---|---|---|
| | 293 K | 303K | 313 K | 323 K |
| Langmuir isotherm | | | | |
| Q0 | 0.625 | 0.943 | 1.02 | 1.52 |
| RL | 0.11 | 0.23 | 0.31 | 0.38 |
| r2 | 0.69 | 0.89 | 0.82 | 0.85 |
| Freundlich isotherm | | | | |
| KF | 50.46 | 16.28 | 11.22 | 8.29 |
| 1/n | 0.495 | 0.507 | 0.523 | 0.444 |
| r2 | 0.95 | 0.99 | 0.98 | 0.98 |

*3.6. Computational study of the adsorption behavior of fish scales.*

3.6.1. Monte Carlo and RDF simulations.

The Monte Carlo simulation was performed to predict both strength and behavior adsorption of ARS onto collagen and HDA surfaces in three media (NM, AM, and BM). It is also possible to obtain the radial distribution function (RDF) (or pair correlation function) G(r).

The RDF is used as a technique to predict the nature of adsorption between ARS and collagen surface/or HDA surface. Modern researchers suggested that the appearance of peaks from 1 Å to 3.5 Å is a sign of chemisorption interactions in nature [47-49]. The stable adsorption interfaces (ARS-collagen/or HDA) are obtained in three media (NM, AM, and BM) and illustrated in Figure 8.
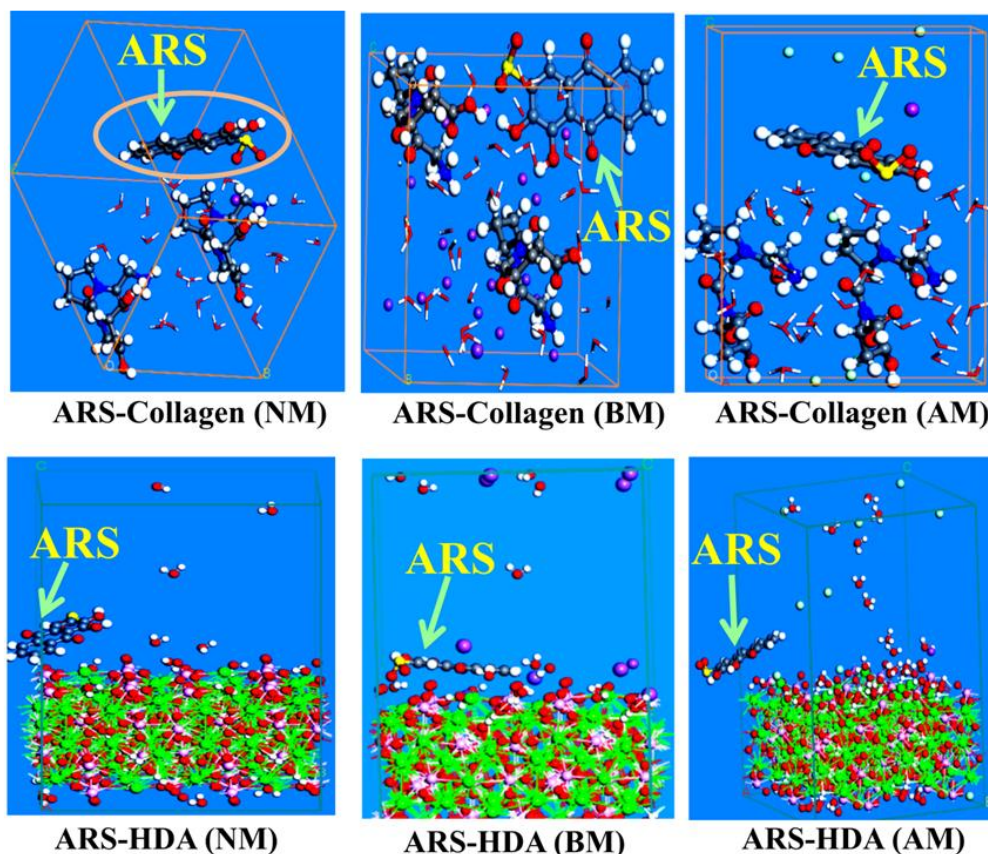


**Figure 8**. Adsorption configurations of ARS on the collagen/ or HDA surface in NM (100H2O), AM (100 H2O, 20 H3O+,20 Cl–), and BM (100H2O,20OH-,20Na+) at a temperature of 297.15 Kelvin and pressure of 1 atm.

To evaluate the adsorption power between ARS and collagen/or HDA a prominent parameter of energy is calculated, such as interaction energy ($E_{int}$) (Table 7) which defines the binding energy of ARS on the collagen/or HDA surface in the three media (NM, AM and BM), this parameter it is commonly recognized to estimate the strength and mechanism of adsorption [50]. As demonstrated in Table 7, it appears that the adsorption of ARS is more favorable on collagen surface than hydroxyapatite mainly in acidic medium, the system of ARS-collagen in acidic media (AM) has a maximum value of $E_{int}$ (194.161 kcal/mol) comparing to the other systems, indicating a stronger interaction between the electron-donating group (−OH and O=C) attached to the benzene ring of ARS and the protonated form of collagen surface. Furthermore, according to these results, we perceived that it was difficult to detach an ARS molecule from the surface when the collagen exists in its protonated form.

**Table 7.** Interaction energy calculated by the Monte Carlo simulation for adsorption of ARS on the collagen/ or HDA surface (in kcal.mol-1) in NM, AM, and BM.

|  | Eint (NM) | Eint (AM) | Eint (BM) |
|---|---|---|---|
| ARS/collagen interface | 190.775 | 194.161 | 181.462 |
| ARS/HDA interface | 161.118 | 156.473 | 162.979 |

RDF plot for the more favored interface (ARS-collagen in AM) was obtained using adsorption Locator modules and forcite field, respectively (Figure 9). The intense peaks of the

RDF analysis correspond to the ARS-collagen in AM system that seems at the link lengths less than 3.5 A°. This result reveals that the adsorption process of the studied system is the chemical adsorption type.
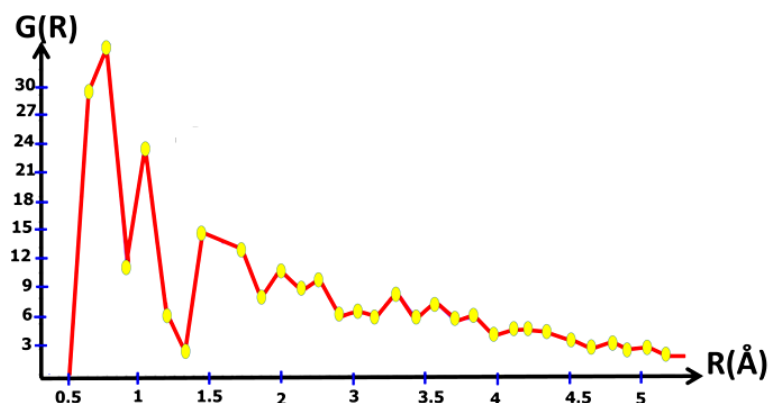


**Figure 9**. Radial distribution function analysis for the more favored interface of adsorption (ARS-collagen in AM)

### 3.6.2. Density functional theory calculations.

#### 3.6.2.1. QP Parameters of structures

The HOMO and LUMO orbitals are a very important tool to describe global reactivity for the systems which containing unsaturated bonds and/or heteroatoms such as oxygen, nitrogen, and sulfur as well as the reactive functional groups, for example, –NH, –N=N–, –C=C–, C=O, –CN, –OH, =S, aromatic moiety, etc. In this respect, a molecule with a higher value of EHOMO, the lower value of ELUMO, and the lower value of ΔEg is more polarizable and generally associated with a high chemical reactivity low kinetic stability. In this study, the calculated QPs aimed to evaluate the global reactivity of ARS and non-protonated form (collagen) and its protonated form (collagen-H+); the QP parameters are exposed in Table 8.

**Table 8.** Calculated QPs.

|  | **EHOMO (eV)** | **ELUMO (eV)** | **ΔEg (eV)** | **μ (eV)** |
|---|---|---|---|---|
| Collagen | -5.83 | -1.21 | 4.62 | -3.52 |
| Collagen-H+ | -7.31 | -4.91 | 2.40 | -6.11 |
| ARS | -5.83 | -2.62 | 3.21 | -4.22 |

As seen in Table 8, the energy gap ΔEg of collagen-H+ has a lower value (ΔEg = 2.40 eV) than that of collagen (ΔEg = 4.62 eV), and that the ARS has a higher global chemical potential concerning that of collagen-H+. These findings clearly indicate the prominent role of the protonation effect for stronger adsorption of ARS towards the collagen-H+ surface. These results are in good correlation with those obtained by the MC study.

#### 3.6.2.2. ESP and MASD analysis.

The depiction of the electrostatic potential surfaces (ESP) has been calculated to define active collagen surface regions. The ESP analysis has been widely used to provide valuable information about the overall molecular charge distribution as well as predicting reactive positions of nucleophilic and/or electrophilic attacks; on which the red color region represents high negative charges of electrostatic potential (EP), the blue color region represents strongly

positive EP. The green region in the ESP surfaces corresponds to a moderate positive charge EP, and the yellow region is a moderate negative charge EP. Figure10 shows the representations of ESP surfaces related to the collagen and collagen-H+.
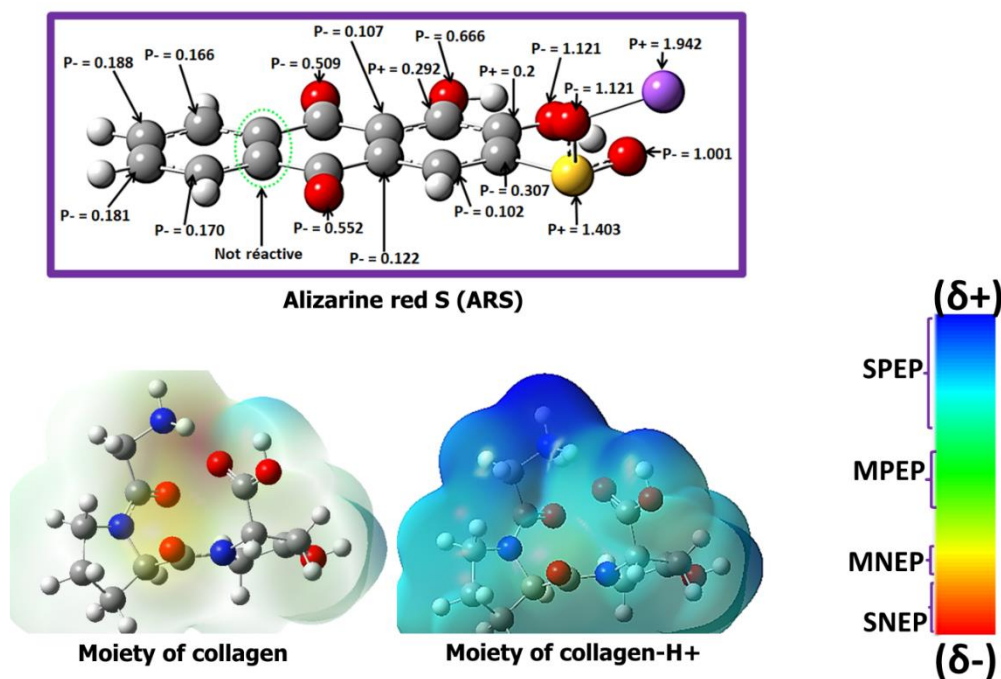


**Figure 10.** Depictions of ESP surfaces for collagen and collagen-H+. Note to ESP plots: Red: Strong negative electrostatic potential (SNEP); Yellow: Moderately negative (MNEP); Blue: Strong positive (SPEP); Green: Moderately positive (MPEP). P- means the nucleophilic Parr indices, and P+ means the electrophilic Parr indices.

The most nucleophilic and electrophilic sites of ARS were evaluated using MASD analysis to calculate nucleophilic Parr indices P− and electrophilic Parr indices P+. These indices are extensively used to give clear information about atomic sites responsible for the nucleophilic and electrophilic interactions, respectively. However, the high values of P− and P+ correspond to the most nucleophilic and electrophilic centers, respectively. Although the atoms were having negative values (or the values close to 0) of P− and P+ would be considered non-reactive atoms. The values of electrophilic P+ and the nucleophilic P− Parr indices are calculated for all atoms of ARS (except the hydrogen atoms) and regrouped in Figure 10. Then, good nucleophilic and electrophilic centers are characterized by maximum P− and P+ values, respectively, and vice versa. We observed that the density of positive charge is mainly located around almost all the surface of collagen-H+; further, we noticed that non-protonated collagen presents both a strong density of the negative charge and a moderate density of positive charge throughout carbon atoms of the benzene ring. This result indicates clearly that the protonated form of collagen (collagen-H+) has strong, active sites when this compound interacts with the ARS molecules by donor-acceptor interaction to form chemical coordination bonds. Similarly, the ESP pictures of collagen and collagen-H+, given in Figure10, show that for both forms, the region of the density of negative charges is slightly distributed at these molecules; suggests the low ability of collagen to donate its electrons to the ARS molecules. Combining with the above results, we concluded that the strong interaction ARS-collagen surface in this study is related to the protonated form of collagen, which results in its high tendency to accept the most nucleophilic atoms (high values of P-) of ARS to form coordinate covalent bonds. Consequently, the collagen-H+ is the appropriate adsorbent to remove ARS molecules from aqueous media.

## 4. Conclusions

Response surface methodology based on a full factorial design model was used to survey the role of adsorption parameters on ARS removal and develop mathematical models for estimating removal efficiency by fish scales. According to thermodynamic studies, the biosorption of anionic dye onto PFS is endothermic, favorable, and spontaneous. The Freundlich isotherm model, which confirms the surface heterogeneity, is the best fit for equilibrium data. The repeating unit Gly-Pro-Hyp was used as the basic unit for the adsorption process. Results of biosorption showed that the adsorption is superior at an acidic medium when the collagen unit takes its protonated form. Monte Carlo, RDF, DFT, and ESP analysis proved that the protonated collagen was the main of the adsorption process and formed a coordinate covalent bond with ARS dye.

## Funding

## Acknowledgments

## Conflicts of Interest

The authors declare no conflict of interest.

## References

1. Anuar, F.I.; Hadibarata, T.; Syafrudin, M.; Fona, Z. Removal of Procion Red MX- 5B from aqueous solution by adsorption on Parkia speciosa (stink bean) peel powder. *Biointerface Res. Appl. Chem*. **2020**, *10*, 4774–4779, https://doi.org/10.33263/BRIAC101.774779.
2. Abdulhameeda, A.S.; Mohammada, A.T.; Jawadb, A.H. Modeling and mechanism of reactive orange 16 dye adsorption by chitosan-glyoxal/TiO2 nanocomposite: application of response surface methodology. *Desalin. and. Water. Treat* **2019**, *164*, 346-360, https://doi.org/10.5004/dwt.2019.24384.
3. Hossain, M.A.; Ali, M.M.; Islam, T.S.A. Comparative adsorption of Methylene Blue on different lowcost adsorbents by continuous column process. *ILCPA* **2018**, *77*, 26-34, https://doi.org/10.18052/www.scipress.com/ILCPA.77.26.
4. Said, B.; Souad, M.; Ahmed, E.H. Classifications, properties, recent synthesis and applications of azo dyes. *Heliyon* **2020**, *6*, https://doi.org/10.1016/j.heliyon.2020.e03271.
5. Mohd, R.; Othman, S. ; Rokiah, H. ; Anees, A. Adsorption of methylene blue on low-cost adsorbents: A review. *J. Hazard. Mater* **2010**, *177*, 70–80, https://doi.org/10.1016/j.jhazmat.2009.12.047.
6. Srivastava, S.; Sinha, R.; Roy, D. Toxicological effects of malachite green. *Aquat Toxicol* **2004**, *66*, 319- 329, https://doi.org/10.1016/j.aquatox.2003.09.008.
7. MegatHanafiah, M.A.K.; MohdJamaludin, S.Z.; Khalid, K.; Ibrahim, S. Methylene blue adsorption on aloe vera rind powder: kinetics, isotherm and mechanisms. *Nature. Environ. Pollut. Technol* **2018**, *17*, 1055–1064.
8. Massoud, K.; Mojtaba, S.; Sahar, M. Removal of Dyes from the Environment by Adsorption Process. *Chem. Mater. Eng* **2018**, *6*, 31-35, https://doi.org/10.13189/cme.2018.060201.
9. Moriguchi, T .; Yano, K. ; Nakagawa, S ; Kaji, A. Elucidation of adsorption mechanism of bone-staining agent alizarin red S on hydroxyapatite by FT-IR microspectroscopy. *J. Colloid Interface Sci* **2003**, *260*, 19−25, https://doi.org/10.1016/S0021-9797(02)00157-1.

10. Jeremić ,S. ; Filipović,N. ; Peulić, A. ; Marković, Z. Thermodynamical aspect of radical scavenging activity of alizarin and alizarin red S, Theoretical comparative study. *Comput. Theor. Chem* **2014**, *1047*, 15−21, https://doi.org/10.1016/j.comptc.2014.08.007.

11. Ghaedi, M. ; Hassanzadeh, A. ; Kokhdan, S. N.  Multiwalled Carbon Nanotubes as Adsorbents for the Kinetic and Equilibrium Study of the Removal of Alizarin Red S and Morin. *J. Chem. Eng. Data* **2011**, *56*, 2511−2520, https://doi.org/10.1021/je2000414.

12. Gholivand, M. B.; Yamini, Y.; Dayeni, M.; Seidi, S.; Tahmasebi, E. Adsorptive removal of alizarin red-S and alizarin yellow GG from aqueous solutions using polypyrrole-coated magnetic nanoparticles. *J. Environ. Chem. Eng* **2015**, *3*, 529−540, https://doi.org/10.1016/j.jece.2015.01.011.

13. Katheresan, V.; Kansedo, J.; Lau, S.Y. Efficiency of various recent wastewater dye removal methods: A review. *J. Environ. Chem. Eng* **2018**, *6*, 4676-4697, https://doi.org/10.1016/j.jece.2018.06.060.

14. Slimani, R.; El Ouahabi, I. ; Abidi, F.; El Haddad, M.; Regti, A.; Laamari, M.R.; Lazar, S. Calcined eggshells as a new biosorbent to remove basic dye from aqueous solutions: thermodynamics, kinetics, isotherms and error analysis. *J. Taiwan. Inst. Chem. Eng* **2014**, *45*, 1578-1587, https://doi.org/10.1016/j.jtice.2013.10.009.

15. Hadibarata, T.; Syafiuddin, A.; Al-Dhabaan, F.A.; Elshikh, M.S.; Rubiyatno. Biodegradation of Mordant orange-1 using newly isolated strain Trichoderma harzianum RY44 and its metabolite appraisal. *Bioproc Biosyst Eng* **2018**, *41*, 621-632, https://doi.org/10.1007/s00449-018-1897-0.

16. Al Farraj, D.A.; Hadibarata, T.; Yuniarto, A.; Syafiuddin, A.; Surtikanti, H.K.; Elshikh, M.S.; Al Khulaifi, M.M.; Al-Kufaidy, R. Characterization of pyrene and chrysene degradation by halophilic Hortaea sp. B15. *Bioproc Biosyst Eng* **2019**, *42*, 963-969, https://doi.org/10.1007/s00449-019-02096-8.

17. El Kassimi, A.; Achour, Y.; El Himri, M.; Laamari, M. R.; El Haddad, M. Optimization of preparation conditions of highly efficient activated carbon for use in water treatment–experimental design approach. *Int. J. Environ. Anal. Chem* **2021**, 1-23, https://doi.org/10.1080/03067319.2020.1861261.

18. El Haddad, M.; Mamouni, R.; Saffaj, N.; Lazar, S. Evaluation of performance of animal bone meal as a new low cost adsorbent for the removal of a cationic dye Rhodamine B from aqueous solutions. *J. Saudi Chem. Soc.* **2016**, *20*, S53-S59, https://doi.org/10.1016/j.jscs.2012.08.005.

19. Regti, A.; El Ayouchia, H. B.; Laamari, M. R.; Stiriba, S. E.; Anane, H.; El Haddad, M. Experimental and theoretical study using DFT method for the competitive adsorption of two cationic dyes from wastewaters. *Appl. Surf. Sci* **2016**, *390*, 311-319, https://doi.org/10.1016/j.apsusc.2016.08.059.

20. Somsesta, N.; Sricharoenchaikul, V.; Aht-Ong, D. Adsorption removal of methylene blue onto activated carbon/cellulose biocomposite films: Equilibrium and kinetic studies. *Mater. Chem. Phys* **2020**, *240*, https://doi.org/10.1016/j.matchemphys.2019.122221.

21. Ribeiro, C. ; Bisinella Scheufele,F. ;Espinoza, F.R. ;Modenes, M. G. ; Carlos da Silva ,M. G. ; Adeodato Vieira, C. E. Characterization of Oreochromis niloticus fish scales and assessment of their potential on the adsorption of reactive blue 5G dye, Colloids .Surf. A Physicochem. Eng. Asp **2015,** 482, 693–701, https://doi.org/10.1016/j.colsurfa.2015.05.057.

22. Ooi,J. ; Lee, L. Y. ; Zhang Hiew, B. Y. ;  Thangalazhy-Gopakumar, Lim.S.S. ; Gan,S. Assessment of fish scales waste as a low cost and eco-friendly adsorbent for removal of an azo dye: Equilibrium, kinetic and thermodynamic studies, *Bioresour. Technol* **2017**, *245*, 656-664, https://doi.org/10.1016/j.biortech.2017.08.153.

23. Uzunogolu,D. ; ozer,A.  Adsorption of Acid Blue 121 dye on fish (Dicentrarchus labrax) scales, the extracted from fish scales and commercial hydroxyapatite: equilibrium, kinetic, thermodynamic, and characterization studies, *Desalination. Water . Treat* **2015**, *57*, 1–23, https://doi.org/10.1080/19443994.2015.1063091

24. Chakraborty,S. ; Chowdhury,S and  Das Saha,P. Fish (Labeo rohita) scales as a new biosorbent for removal of textile dyes from aqueous solutions, *J. Water Reuse Desalination* **2012,** *2*, 175-184, https://doi.org/10.2166/wrd.2012.074.

25. Fijul Kabir,S.M. ; Cueto,R. ; Balamurugan,S. ;  Romeo,L.D. ; Kuttru,J.T. ; Marx Ioan, B.D. ; Negulescu,I. Removal of Acid Dyes from TextileWastewaters Using Fish Scales by Absorption Process, *clean technol.* **2019**, *1*, 311–325, https://doi.org/10.3390/cleantechnol1010021.

26. Muhammad,N, ;Gao,Y. ;Iqbal,F. ; Ahmad,P. ; Ge,R. ; Nishan,U. ; Rahim,A. ; Gonfa,G. ; Ullah,Z. Extraction of biocompatible hydroxyapatite from fish scales using novel approach of ionic liquid pretreatment, *Sep. Purify. Technol* **2016,** *161*, 129-135, https://doi.org/10.1016/j.seppur.2016.01.047.

27. Glanville,R .W. ; Breitkreutz,D. ; Meitinger,M. ; Fietzek,P.P. Completion of the amino acid sequence of the α1 chain from type I calf skin collagen. Amino acid sequence of α1(I)B8, *Biochem. J* **1983** , *215*, 183–189, https://doi.org/10.1042/bj2150183.

28. Eastoe, J. E. The amino acid composition of mammalian collagen and gelatin, *Biochem. J* **1955** , 61, 589–600, https://doi.org/10.1042/bj0610589.

29. Gaussian 09. Revision D. 01, Frisch, M. J. et al, Gaussian, Inc., Wallingford CT) **2009**

30. Tighadouini,S. ; Radi,S. ; El Massaoudi,M. ; Lakbaibi,Z. ;Ferbinteanu,M. ;Garcia,Y. Efficient and Environmentally Friendly Adsorbent Based on β-Ketoenol-Pyrazole-Thiophene for Heavy-Metal Ion Removal from Aquatic Medium: A Combined Experimental and Theoretical Study. *ACS Omega* **2020**, *5*, 17324-17336, https://doi.org/10.1021/acsomega.0c01616.

31. Hariharan, P. C. ; Pople, J. A. The influence of polarization functions on molecular orbital hydrogenation energies, *Theor. Chem. Acta* **1973**, *28*, 213-222, https://doi.org/10.1007/BF00533485

32. Benallou, A. ; Lakbaibi,Z. ; Garmes,H. ; El Abdallaoui, H.E.A. The role of the polarity on the mechanism and selectivity in the [3+ 2] cycloaddition reaction between CF3-ynone ylide and azide group: A quantum chemical investigation, *J. Fluor. Chem* **2019**, *219*, 79-91, https://doi.org/10.1016/j.jfluchem.2018.12.008

33. Hsissou, R.; Benzidia,B.; Hajjaji, N.; Elharfi, A .Elaboration, electrochemical investigation and morphological study of the coating behavior of a new polymeric polyepoxide architecture: crosslinked and hybrid decaglycidyl of phosphorus pentamethylene dianiline on E24 carbon steel in 3.5% NaCl. *Electrochim. Acta* **2019**, *37* ,179-191, http://dx.doi.org/10.4152/pea.201903179.

34. Lakbaibi, Z.; Abou El makarim,H.; Tabyaoui, M.; EL Hajbi, A. Study of the solvent effects on the formation of α-bromoglycidic esters in aliphatic series using the quantum DFT method with B3LYP/6-311G (d, p). *J. Mater. Environ. Sci* **2016**, *8*, 99-115.

35. Jaafar, A.; Ben El Ayouchia, H.; Lakbaibi, Z.; Boussaoud, A.; Jodeh, S.; Azzaoui, K.; Tabyaoui, M. Degradation of Pollutant Dye in Aqueous Solution using Fenton Reaction: A DFT Study. *G P Globalize Research Journal of Chemistry* **2019**, *3* ,53-61.

36. Manssouri, M.; Lakbaibi, Z.; Znini, M. Impact of Aaronsohnia pubescens Essential Oil to Prevent Against the Corrosion of Mild Steel in 1.0 M HCl: Experimental and Computational Modeling Studies. *J. Fail. Anal. Prev* **2020**, https://doi.org/10.1007/s11668-020-01003-8.

37. Sun, H. COMPASS: An ab initio force-field optimized for condensed-phase applications overview with details on alkane and benzene compunds, J. Phys. Chem. B **1998**,102, 7338-7364 https://doi.org/10.1021/jp980939v.

38. Kara, A. ; Tamburaci, S.; Tihminlioglu, F.; Havitcioglu, H. Bioactive fish scale incorporated chitosan biocomposite scaffolds for bone tissue engineering, *Int. J. Biol. Macromol* **2019,** *130*, 266-279, https://doi.org/10.1016/j.ijbiomac.2019.02.067

39. Bose, S. ; Saha, S.K. Synthesis and characterization of hydroxyapatite nanopowders by emulsion technique. *Chem. Mater* **2003**, *15* ,4464-4469. https://doi.org/10.1021/cm0303437

40. Wang, Y. ; Liu, T. ; Yan,Y. ; Li,S. Comparative study on lattice parameters of HAP nanoparticles with those of HAP whiskers, *J. Wuhan Univ. Technol. Mater. Sci. Ed.* **2008,** *23*, 395-398, https://doi.org/10.1007/s11595-007-3395-0.

41. Khataee, A.R. ; Zarei, M. ; Ordikhani-Seyedlar, R. Heterogeneous photocatalysis of a dye solution using supported TiO2 nanoparticles combined with homogeneous photoelectrochemical process: Molecular degradation products. *J. Mol. Catal. A: Chem* **2011**, *338* , 84-91, https://doi.org/10.1016/j.molcata.2011.01.028

42. Soltani, R.D.C. ; Rezaee, A. ; Godini,H. ; Khataee, A.R. ; Hasanbeiki, A. Photoelectrochemical treatment of ammonium using seawater as a natural supporting electrolyte. *Chem. Ecol* **2013**, *29*, 72-85, https://doi.org/10.1080/02757540.2012.704913.

43. Bello, O.S.; Fatona, T.A.; Falaye, F.S.; Osuolale, O.M.; Njoku, V.O. Adsorption of eosin dye from aqueous solution using groundnut hull–based activated carbon: kinetic, equilibrium, and thermodynamic studies. *Environ. Eng. Sci* **2012**, *29*, 186-194, https://doi.org/10.1089/ees.2010.0385.

44. Singh, N.B.; Nagpal, G.; Agrawal, S.; Rachna,N. Water purification by using Adsorbents: A Review. *Environ. Technol. Innov* **2018**, *11*, 187–240, https://doi.org/10.1016/j.eti.2018.05.006.

45. Weber, T.W.; Chakravorti, R.K. Pore and solid diffusion models for fixed-bed adsorbers. *AIChE Journal* **1974**, *20*, 228-238, https://doi.org/10.1002/aic.690200204.

46. Satlaoui, Y.; Nasraoui, R.; Charef, A.; Azouzi, R. Adsorption, Modeling, Thermodynamic, and Kinetic Studies of Methyl Red Removal from Textile-Polluted Water Using Natural and Purified Organic Matter Rich Clays as Low-Cost Adsorbent. *J. Chem* **2020,** https://doi.org/10.1155/2020/4376173.

47. Lakbaibi ,Z. ;Jaafar,A. ; Ben El Ayouchia ,H. ; Tabyaoui ,M. and Boussaoud, A. Reactivity and mechanism of nucleophilic addition reaction of amine with alkene: A systematic DFT study. *Mediterr. J. Chem* **2019**, 8, 25-29, http://dx.doi.org/10.13171/mjc811902924zlhbea.

48. Manssouri, M. ; Lakbaibi, Z. ; Znini, M. Impact of Aaronsohnia pubescens Essential Oil to Prevent Against the Corrosion of Mild Steel in 1.0 M HCl: Experimental and Computational Modeling Studies. *J Fail Anal Prev* **2020**, *20*, 1939-1953, https://doi.org/10.1007/s11668-020-01003-8.

49. Manssouri, M. ; Znini, M.. ; Lakbaibi, Z. Experimental and computational studies of peril aldehyde isolated from Ammodaucus leucotrichus essential oil as a green corrosion inhibitor for mild steel in 1.0 M HCl. *Chem. Pap* **2020**, 75, 1103-1114, https://doi.org/10.1007/s11696-020-01353-5.

50. Ansari,A. ; Lakbaibi,Z. ; Znini,M. ; Manssouri,M. ; Laghchimi, A. Evaluation of Corrosion Inhibition and Adsorption Behavior of 7-Isopropyl-4-methyl-4,5,6,7-tetrahydrobenzoisoxazole against Carbon Steel Corrosion in 1 M HCl. Experimental and Computational Investigations. *Anal. Bioanal. Chem. Res* **2021**, *8*, 113-128, https://doi.org/10.22036/ABCR.2020.233677.1509.